# A SOFT GLOVE: DESIGN, MODEL, FABRICATION, AND sEMG-BASED CONTROL EXPERIMENTS

Huadong Zheng,* Yongfeng Tian,** Yan Cheng,** Caidong Wang,** Ayong Li,** Xinjie Wang,** Fengyang Liu,*** and Liangwen Wang**

## Abstract

Unlike prior designs of sot robots with only one actuator per finger, this study designed and built a soft glove with multiple soft actuators on one finger to address current problem of soft hand robots lack of flexibility. Soft glove can help patients with loss of hand motor function in rehabilitation training and object grasping. Firstly, the 3D model of soft glove is established, and the motion of soft finger is analysed by finite element. The soft finger prototype was then created using 3D printing and casting method. Secondly, an experimental platform for measuring the soft actuator's output force was created, and the soft actuator's output force capability was evaluated. Then, soft finger movement experiments were used to confirm the structure's practicality. The simulation model's accuracy was confirmed by comparing statics simulation data with soft finger experimental data. Thirdly, a control experimental platform was employed to implement mirror therapy, and surface electromyography (sEMG) signals were used to allow patients to complete mirror therapy while wearing soft glove. Finally, the gripping ability of soft glove was demonstrated by successfully grasping of things varying in weight, shape, and size. Soft glove assisted humans in grasping objects in various ways, proving that it could help patients grip objects more flexibly.

## Key Words

Soft glove, actuator, soft fingers, finite element analysis, mirror control

## 1. Introduction

Soft robots can be operated more safely and conveniently in unstructured environments because of the soft character of the material. Soft grippers and soft hands, for example, are commonly employed in industrial, medical treatment, bionics, and other disciplines [1]. Soft robots and devices, as opposed to typical rigid robots, can conduct desired interactions or activities in unstructured situations due to their inherent flexibility, stretchability, and conformability [2]. Hence, the inception of soft robots shifts the paradigm and trends in robotics, which could potentially revolutionise related applications [3]. Various new and diverse soft structures have appeared in the development of soft robots to suit the space needs of particular working situations. As a result, more demands are placed on soft robot manufacturing technologies [4]. Soft robots are traditionally produced by casting silicone rubber materials [5]. Traditional manufacturing technology has been unable to meet the moulding requirements of varieties of soft robots with complex structures [6], so a new method based on textile materials processing or flexible materials 3D printing has emerged to solve the problem of complex model manufacturing difficulties [7]. The emergence of functional soft materials has also facilitated the development of soft actuators and artificial muscles that can remotely control soft materials through external stimuli [8]. In addition, a threadlike robot based on magnetic materials has been developed to navigate through narrow and complex cerebral vessels [9].

Researchers have designed and built many biomimetic robots using the bending capabilities of soft actuators, including octopus-inspired soft robot [10], soft frog-inspired swimming robot [11], soft robot bioinspired by Venus flytrap [12], lobster-inspired robotic glove [13], and soft-bodied robots inspired by Honeycomb PneuNets (HPN) [14]. Soft robots hold great promise for many important applications, especially in the biomedical field, where their inherent mechanical compliance improves the safety of handling and provides a new approach to the rehabilitation of patients with hand dysfunction [15]. As a result, researchers created a pneumatic soft robot to assist stroke patients with hand rehabilitation training [16]. Soft robotic therapy is more convenient and intelligent than previous manual rehabilitation methods and can provide real-time data feedback during treatment to optimise the patient's treatment plan [17].

* Henan Key Laboratory of Intelligent Manufacturing of Mechanical Equipment, Zhengzhou University of Light Industry, Zhengzhou, China
** Department of Mechanical Engineering, Zhengzhou University of Light Industry, Zhengzhou, China
*** School of Electrical and Information Engineering, Zhengzhou University of Light Industry, Zhengzhou, China
Corresponding author: Huadong Zheng

*Recommended by Jason Gu*
*(DOI: 10.2316/J.2024.206-1065)*

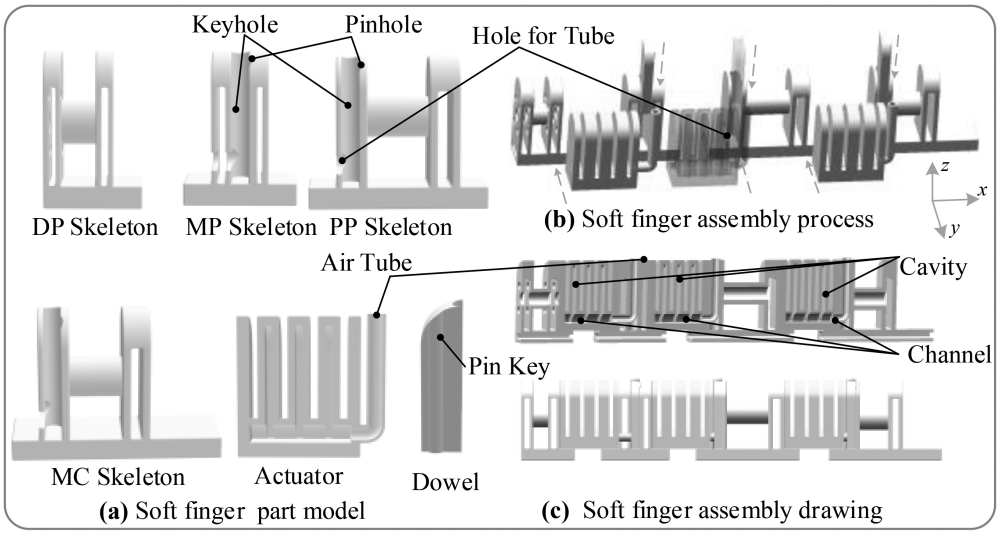


Figure 1. Diagram of the soft finger assembly structure.

During the investigation, researchers tested a variety of approaches to achieve soft glove fabrication, including rope actuation, smart materials or polymers, and pneumatic actuators [18]. However, rope-actuated soft gloves still have a stiff structure, and the actuation effect of polymer-based soft gloves is considerably inferior to that of soft actuators. As a result, the structure of soft gloves is still primarily made up of soft actuators. Yap *et al.* designed a soft glove powered by air pressure, fabricated a prototype of the soft finger out of silicone rubber, and analysed the relationship between the input pressure and the soft glove's curvature. Based on this, the team also took advantage of the anisotropy of textiles to develop a soft finger structure in which a fibrous textile wraps soft rubber. In research of fiber-reinforced pneumatic muscle, Al-Fahaam *et al.* [19] and Alibadi and Davis [20] designed and manufactured a pneumatic muscle actuator based on McKibben artificial aerodynamic muscles. The structure of pneumatic muscle is formed by wrapping a cylinder of silicone rubber in a fibrous fabric. Pneumatic muscles can flex over 500 degrees. The fiber fabric wrapped around the pneumatic muscle also effectively improves its carrying capacity. Cappello *et al.* designed a soft glove structure with pleated features. They improved the driving force of the finger bending motion by focusing the folds on finger joints.

Based on the above research, this paper proposes a new soft glove robot structure composed of multiple soft actuator fingers. The soft glove, which is based on human hand's joint anatomy, can drive a single joint or many joints of human finger. This paper is structured as follows: Section 2 explained the design inspiration of the soft glove and describes the overall 3D structure of soft glove, as well as the assembly relationship and size information of soft finger. In Section 3, the statics analogue model of the soft finger is first presented and the fabrication process of the soft finger is described. Then the output force capability of the soft actuator is measured. Finally, the static simulation results of the soft finger are compared with the experimental results. Section 4 set up an experimental platform to control soft glove by surface electromyography (sEMG) signal and verify the ability of soft glove to assist patients in grasping and recovery performance through experiments.

## 2. The Structure of Single Finger

Based on the structure of the human hand, the fingers of soft glove have flexibility of up to three degrees of freedom, enabling soft finger to imitate different movements of the human hand. The human hand is made up of distal phalanges (DP), middle phalanges (MP), proximal phalanges (PP), metacarpals (MC), metacarpophalangeal joints (MP), proximal interphalangeal joints (PIP), and distal interphalangeal joints (DIP), the soft glove is made up of an MC skeleton, a PP skeleton, an MP skeleton, a DP skeleton, and many soft actuators that operate as revolute joints to connect the skeletons.

The hard resin material (SOMOS Imagine 8000) and soft silicone rubber material (Dragon Skin 30) [21] make up the soft glove. Soft actuators, for example, are made up of separate channels and chambers. Each section of the soft finger is fitted with the same soft actuator, which helps to improve the control precision of soft finger joint bending. Simultaneously, each soft actuator is independently attached to the outside air tube, allowing the soft glove to do a wide range of actions that a human hand can perform. The single finger schematic is shown in Fig. 1. On each skeleton, there are not just holes for tubes to flow through but also pin holes for dowels to be placed. Furthermore, the skeleton and actuator are linked and secured by glue upon that side of the soft actuator without an external tube and on the side where the bottom of the soft actuator was in touch with the skeleton.

The designed parameters for the soft glove are summarised in Table 1. According to the content of literature [22], for wearing comfortable, weight and overall dimension of the soft glove are suggested within 300 g and 180 mm × 140 mm × 30 mm, respectively.

The size of the glove can be adjusted by changing the parameters of the actuator and the skeleton,

Table 1
The Designed Parameters of Soft Glove ($x \times y \times z$)

| Name | Size / (mm × mm × mm) | Weight / (g) |
|---|---|---|
| Actuator | 20×12×23 | 7.21 |
| SGT(soft glove thumb) | 110×12×23 | 23 |
| SGIF(soft glove index finger) | 142×12×23 | 34 |
| SGMF(soft glove middle finger) | 152×12×23 | 36 |
| Soft gloveF(soft glove ring finger) | 142×12×23 | 34 |
| SGLF(soft glove little finger) | 134×12×23 | 31 |
| MC Skeleton | 38×12×23 | 2.86 |
| SGT PP Skeleton | 32×12×23 | 3.83 |
| SGMF PP Skeleton | 40×12×23 | 5.85 |
| SGLF PP Skeleton | 30×12×23 | 2.76 |
| Other finger PP Skeleton | 32×12×23 | 4.98 |
| SGMF MP Skeleton | 24×12×23 | 3.03 |
| SGLF MP Skeleton | 16×12×23 | 2.03 |
| Other finger MP Skeleton | 22×12×23 | 2.75 |
| DP Skeleton | 20×12×23 | 2.21 |
| Soft glove | 152×60×23 | 158 |

allowing patients to choose the suitable size of the glove according to their hand size. According to the physician's recommendations, the actuator must aid patients with at least 225 degrees of finger flexion and 1.5 N of finger-tip force during hand rehabilitation. Then, the bending ability of soft finger and the actuator's output force ability will be evaluated below.

## 3. Simulation Analysis and Experimental Verification of Soft Finger

### 3.1 Hyperelastic Material Parameters

Because of the nonlinear characteristics of hyperelastic materials, it is sometimes difficult to calculate the mechanical parameters of the materials accurately. Add some basic assumptions to soft materials to better conduct theoretical research. First, assume that the material is isotropic and incompressible. Then established the hyperelastic constitutive model of rubber material built on the stress–strain relationship using phenomenological theory. Figure 2, The curves depict the uniaxial and biaxial tensile experiments under five theoretical models. The second-order three-term Mooney-Rivlin model exhibits a more accurate fit; hence, this paper adopts the Mooney-Rivlin theoretical model. The strain energy function can be expressed as:

$$W = W(I_1, I_2, I_3) \tag{1}$$

where $W$ is the strain energy density, $I_1, I_2,$ and $I_3$ are the three invariants of the Green deformation tensor given in terms of the principal extension ratios $\lambda_1, \lambda_2,$ and $\lambda_3$ by:

$$\begin{cases} I_1 = \lambda_1^2 + \lambda_2^2 + \lambda_3^2 \\ I_2 = \lambda_1^2\lambda_2^2 + \lambda_1^2\lambda_3^2 + \lambda_2^2\lambda_3^2 \\ I_3 = \lambda_1^2\lambda_2^2\lambda_3^3 = 1 \\ \lambda_i = 1 + \gamma_i \end{cases} \tag{2}$$

Where $\gamma_i$ is the principal strain. For incompressible materials, $I_3 = 1$, (1) reduces to:

$$W\left(I_1, I_2\right) = \sum_{i,j=0}^{n} C_{\mathrm{ij}}(I_1 - 3)^i + (I_2 - 3)^j \tag{3}$$

The binomial third-order expansion of the Mooney–Rivlin model is as follows:

$$W = C_{10}\left(I_1 - 3\right) + C_{01}(I_2 - 3) \tag{4}$$

where $C_{10}$ and $C_{01}$ are the material constants to be solved.

According to Kirchhoff stress tensor and Green strain tensor, $\sigma_2 = \sigma_3 = 0,\ \lambda_2^2 = \lambda_3^2 = \frac{1}{\lambda_1}$, through the stretching experiment, the relation between the principal stress and the principal elongation ratio of rubber is:

$$\sigma_1 = 2\left(\lambda_1^2 - \frac{1}{\lambda_1}\right)\left(\frac{\partial W}{\partial I_1} + \frac{1}{\lambda_1}\frac{\partial W}{\partial I_2}\right) \tag{5}$$

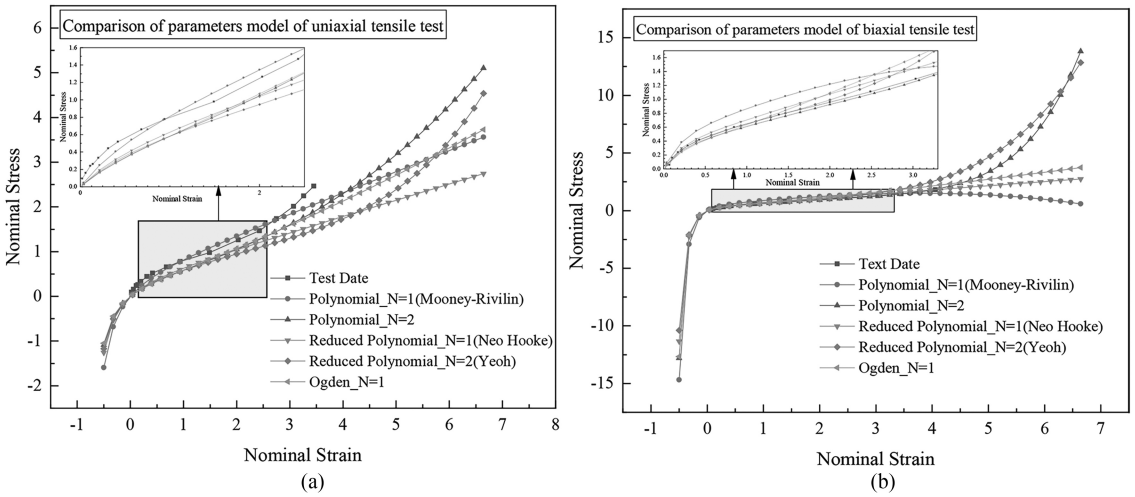


Figure 2. Results of tensile tests on hyperelastic materials and stress–strain analysis of various constitutive models of hyperelastic materials.

From (7):

$$\frac{\partial W}{\partial I_1} = C_{10}, \frac{\partial W}{\partial I_2} = C_{01} \tag{6}$$

Combining (8) with (9) gives the relations:

$$\frac{\sigma_1}{2(\lambda_1^2 - \frac{1}{\lambda_1})} = C_{10} + \frac{1}{\lambda_1} C_{01} \tag{7}$$

In the tensile test, we obtained the relationship between principal stress and principal elongation ratio and then fit the data. Setting $\frac{1}{\lambda_1}$ as the $x$-coordinate and $\frac{\sigma_1}{2(\lambda_1^2 - \frac{1}{\lambda_1})}$ as the $y$-coordinate. The slope of the fitted line is $C_{01}$ and the intercept is $C_{10}$. By the dumb-bell tensile experiment, the parameters data can be solved as follows: $C_{10} = 0.172$, $C_{01} = -0.023$, and then we use ABAQUS software to analyze the model through the parameters obtained above.

### 3.2 Soft Finger Simulation Model

ABAQUS was used to evaluate the static motion of the soft finger model. Changing the internal pressure of each actuator chamber of the soft finger during the analysis yielded the model's deformation effect under various pressure settings. Fig. 3 depicts the precise procedure.

The constraint conditions between the soft actuator and each skeleton were first set as binding constraints, then the soft actuator's contact surface was set as slave surface, and the skeleton's contact surface was set as master surface, according to the design requirements of soft finger. The soft actuator's interaction property between chambers was set to contact. The fluid cavity points and cavity surfaces were located within the soft actuator cavity, as illustrated in Fig. 3(b).

Boundary conditions of MC Skeleton were set as fixed constraints, and the soft finger model was meshed, as shown in Fig. 3(c). Because each skeleton has regular characters, the element type in the mesh partition was selected as hexahedron and the irregular shape of soft actuator was selected as a tetrahedron. To ensure that the mesh size of the slave surface was smaller than that of the main surface, the approximate global seeds size of the soft actuator was set to 0.8 and the global seeds layout of the skeleton was set to 1.0. The final simulation results are shown in Fig. 3(d). The coefficients of Mooney–Rivlin strain energy potential are shown in Table 2 and the mechanical parameters of the skeleton material are shown in Table 3, which include $E$ (modulus of elasticity), $\lambda$ (Poisson's ratio), and $\rho$ (density).

Table 2
The Coefficients of Mooney-Rivlin Strain Energy Potential

| Coefficients | $C_{10}$ | $C_{01}$ | D1 |
|---|---|---|---|
| Value | 0.234 | −0.0033 | 0 |

Table 3
Mechanical Parameters of Skeleton Material

| Coefficients | E / (MPa) | $\lambda$ | $\rho$ / (g/cm$^3$) |
|---|---|---|---|
| Value | 2.32 | 0.3902 | 1.2 |

### 3.3 Design of Actuator Mould and Fabrication of Soft Finger

The convenience of casting and demoulding should be considered before designing the mold. Therefore, detachable modules are used to form the mold of the soft actuator shown in Fig. 4(a). The skeleton and the mould of the soft actuator are made by 3D printing technology. From Fig. 4(b), to prevent the vulcanisation failure of silicone rubber, nylon material is used as the material of the mold. During the manufacturing process, place the mould filled with liquid silicone rubber in an incubator and set the temperature to 60°C to speed up the molding of the soft actuator. In around 3–4h, a thermostatic actuator can complete the vulcanisation reaction. It is a great technique to save material by finishing the bottom of the soft actuator

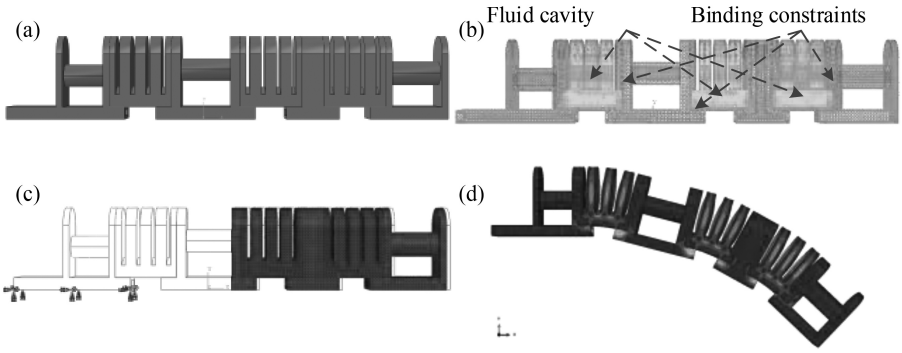


Figure 3. Static simulation of soft finger.

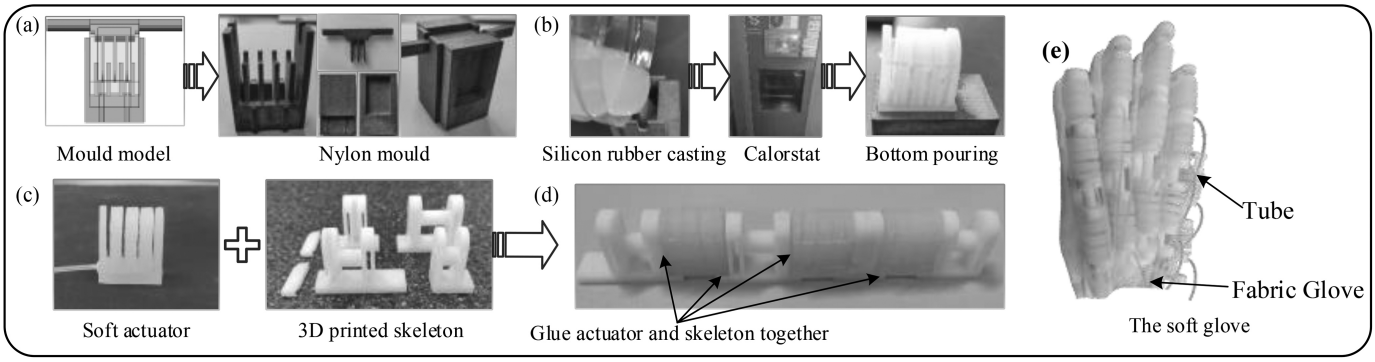


Figure 4. The fabrication process of soft finger.

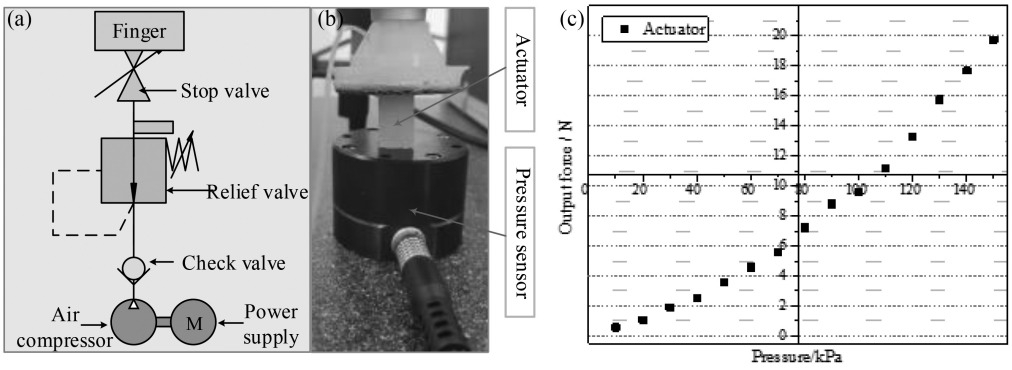


Figure 5. Measuring platform for the output force of the actuator.

with the grooves from the mould module. Fig. 4(c) depicts the completed soft actuator and skeleton, while Fig. 4(d) shows a complete soft finger.

### 3.4 Experiment with Soft Actuator Output Force

It is vital to determine if the soft glove can provide appropriate grasping power when it is utilized to assist patients with rehabilitation treatment or gripping objects. However, the grabbing force of soft glove is very minimal compared to regular rigid gloves, and the deformation of soft actuators is nonlinear, making it difficult to solve the actuator's output force using theoretical approaches. Thence, experimentation is used to determine the soft actuator's output force.

As shown in Fig. 5, a test platform for soft actuator output force was built. Before the signal acquisition, the pneumatic circuit system shown in Fig. 5(a) was built to provide air pressure to the soft actuator. Fig. 5(b) depicts the output force signal acquisition platform. A 6-axis force load cell (Force Sensor Smart_100. Capacity, 0–100 N) was used to collect the output force signal of the soft actuator. Fig. 5(c) shows the soft actuator's output force at various pressures.

The soft glove safety as a patient-wearable device must be thoroughly examined, so the soft drive's maximum pressure tolerance was tested. The soft glove can function normally when the soft actuator's input pressure is stable at 150 kPa. The soft actuators will explode if the input pressure exceeds 160 kPa. Fig. 5(c) also shows that the maximum output pressure of the soft

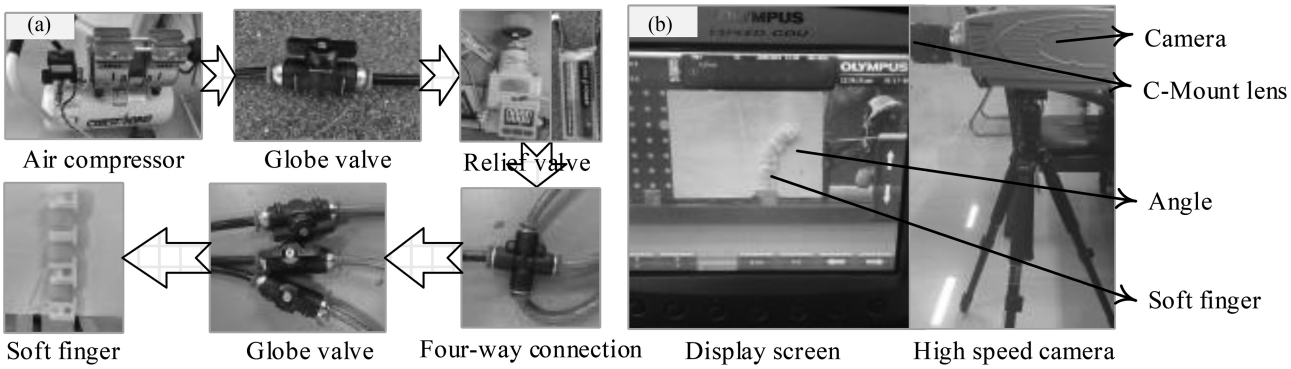


Figure 6. Soft finger movement's experimental platform.

actuator is 19.83 N at the maximum input pressure of 150 kPa.

### 3.5 Construction of Soft Finger Movement Experiment Platform.

As shown in Fig. 6(a), the power producer of the coupled finger is composed of an air compressor, globe valve, relief valve, and four-way connection. A high-speed camera is employed to record the movement process of the connected finger to examine the entire moving process. A high-speed camera consists of a camera, a C-port lens, a stand, and a display screen. In the process of image acquisition, the motion of the soft finger is photographed at a speed of 60 frames per second (fps), and 60 motion pictures can be obtained per second to ensure accurate motion data can be obtained.

### 3.6 Comparison of Soft Finger Simulation Results and Experimental Results

The simulation results of the soft finger, as illustrated in Fig. 7, can accurately depict the precise movement process of the real object. According to the literature, the maximum bending angle of the human finger MP joint, PIP joint, and DIP joint is 90 degrees, 100 degrees, and 80 degrees, respectively. During the experiment, when the air pressure reached 80 kPa, the bending angle of MP joint of the soft finger has reached 90.8 degrees, and the bending angle of DIP joint has reached 91.9 degrees, both higher than the maximum angle of human finger bending. Although the soft finger's PIP bending angle is 89.3 degrees at 80 kPa, which is less than the maximum angle of human finger bending, the PIP bending angle of soft finger will also reach 100 degrees at air pressures greater than 90 kPa. As can be seen in Fig. 7(b), the bending angle of soft finger at the DIP is 11.9 degrees, higher than the maximum bending angle of the human finger but 0.1 degrees lower than the simulation results at 80 kPa air pressure. The MP joint of soft finger is only 0.8 degrees higher than the maximum angle of hand bending but 1 degree lower than the simulation results. Although the PIP joint of soft finger is 10.7 degrees, lower than the maximum angle of hand bending, it is also 1.9 degrees lower than the simulation results. However, it can still exceed the maximum angle of hand bending when the air pressure exceeds 90 kPa.

The simulation findings at the three joints of soft finger were compared with the experimental results, as shown in Fig. 7(c), to validate the accuracy of the simulation data, and reasons for the mistakes were also analysed.

To lower the overall weight of soft glove, not only was lightweight material used for each skeleton but the structure was also optimised to obtain a light glove. Each light skeleton has little effect on the soft actuator's bending deformation in the experiments, therefore the static motion of soft finger at the three joints produces very similar results. Fig. 7(d) shows the comparison between simulation and experimental data. The largest error is 2.7 degrees, while the average error between the MP joint simulation results and the experimental findings is 1.21 degrees. For PIP joints, the average discrepancy between simulation and experimental results is 1.4 degrees, with the maximum error of 3.5 degrees. The average error between the DIP joint experiment and simulation results is 1.04 degrees, and the maximum error is 1.4 degrees. The actuator error at DIP is minimal, which is also attributable to the fact that the actuator at DIP is only attached to the DP skeleton and encounters the least resistance. Not only can the soft glove lightweight design method effectively minimise the difference between simulation and experiment, but it can also effectively reduce the difference between each joint bending angle. As a result, managing each joint actuator can reduce the control difficulty of driving finger movement, allowing it to meet the goal of controlling the soft glove with a simple control strategy. The data obtained from the experiment and simulation results are also helpful to guide and control the input of experimental air pressure and realise the bending of each joint of the soft finger at a given angle.

## 4. Control of Soft Glove Via sEMG

### 4.1 sEMG-based Control Experiments

Mirror therapy is used to help stroke patients achieve rehabilitation by wearing soft glove. Mirror therapy is to collect movement of the finger on the normal side of patient to achieve the same movement of the affected finger. Fig. 8 is a control platform for patients to perform mirror therapy through the collection, analysis, and reading

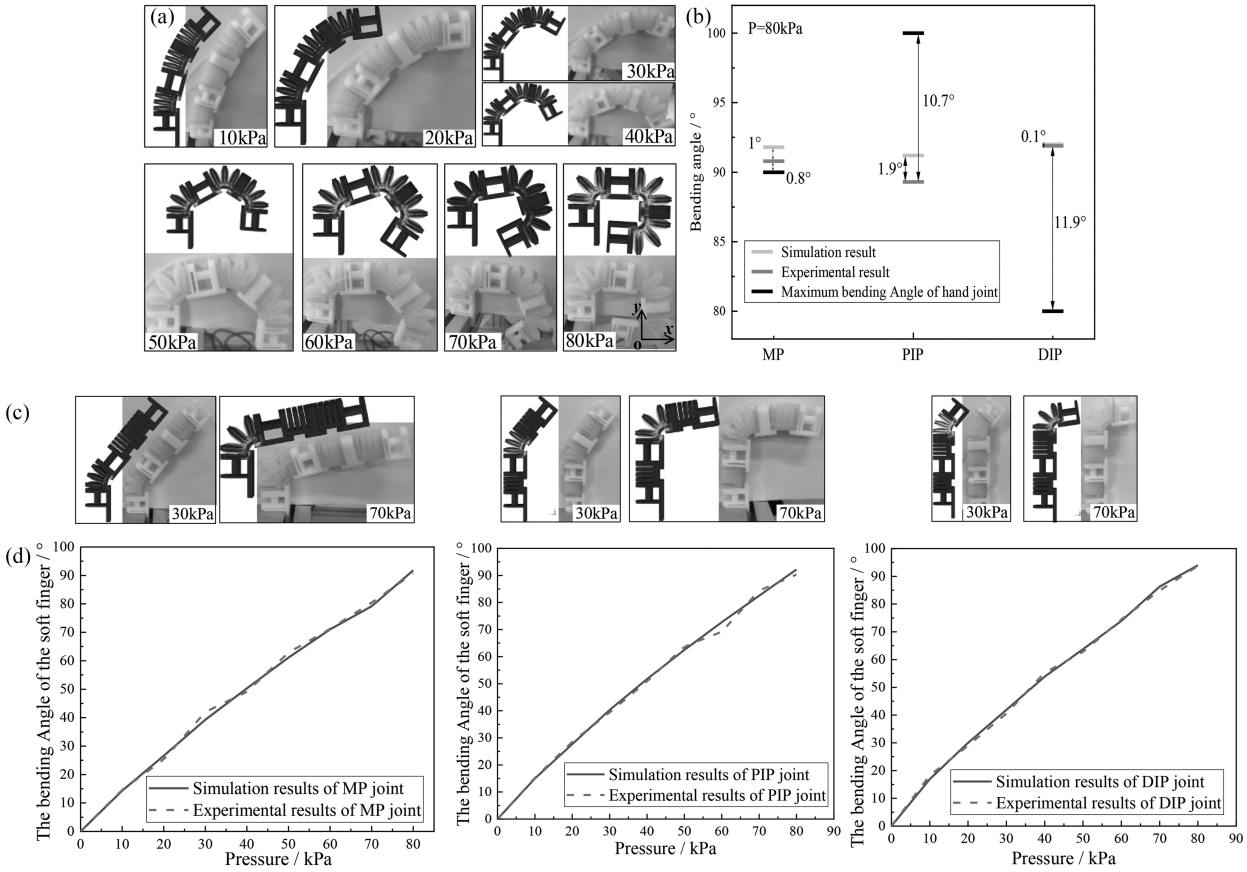


Figure 7. The bending angles of the simulation and experimental results are compared at the three joints of the finger.

of EMG signals. The control platform is composed of the signal circuit, electric circuit, and pneumatic circuit system.

Electrode patches affixed to the arm are used to capture EMG data. To complete the first filtering and amplification procedure, the original EMG signal is sent to the sensor. The signal is then fed into the computer for further processing, amplification, and detection of signal properties. Then, using the Bluetooth module, create a link between the sensor and the control board to complete the signal transmission. The signal is sent from the control board to the relay module through the breadboard. The relay module is responsible for the on–off of the circuit and the commutation of the control solenoid valve. The output of pneumatic pressure at different ports of the solenoid valve drives the brake on the soft glove. In this way, soft glove can then mimic the movements of the healthy side fingers, allowing mirror therapy to be performed. In the experiment, six gestures, namely, thumb flexion, index finger flexion, middle finger flexion, ring finger flexion, little finger flexion, and fist-clenching were tested, respectively, as shown in Fig. 9.

When the finger rests, the sEMG signal is smooth. Once the finger flexes, after the controller recognises the gesture, the relevant pins of the controller will output a high level to the relay module to turn on the circuit. The corresponding solenoid valve starts to work to realise the same flexion action of the soft finger corresponding to the flexion of the human finger.

The sEMG signal generated by a finger flexion and extension is very weak, so the signal generated by a finger joint flexion and extension will be even weaker, which brings great challenges to improve the accuracy of control.

Although the flexion and extension control of one soft glove finger has been realised at present, the accuracy of signal acquisition and processing will continue to be optimised in the future, and the electric proportional valve will be combined to achieve more precise control of each joint.

### 4.2 Grasp Experiment

As can be seen in Fig. 10(a) (i), the total weight of the soft glove is 158 g. In subsequent experiments, the ability of the soft glove to grasp objects and assist patients to grasp objects was studied. It can be seen in Fig. 10(a) (ii)–(vi) that the soft glove can not only grasp the apple with the maximum weight of 298.38 g but also grasp the scissors with the weight of 47.39 g.

In Fig. 10(b), when the soft glove assisted patients to grasp objects, the grasping of apples, tape, and mugs with large mass was achieved by using the full drive method. For the signature pen, U disk, four-way connection, and other small mass objects, only a few joints of the thumb and index finger can be realised. This shows that soft glove with multiple drives provides more diversity in grasping functions. It can also avoid the movement of the whole finger when traditional soft gloves grab.

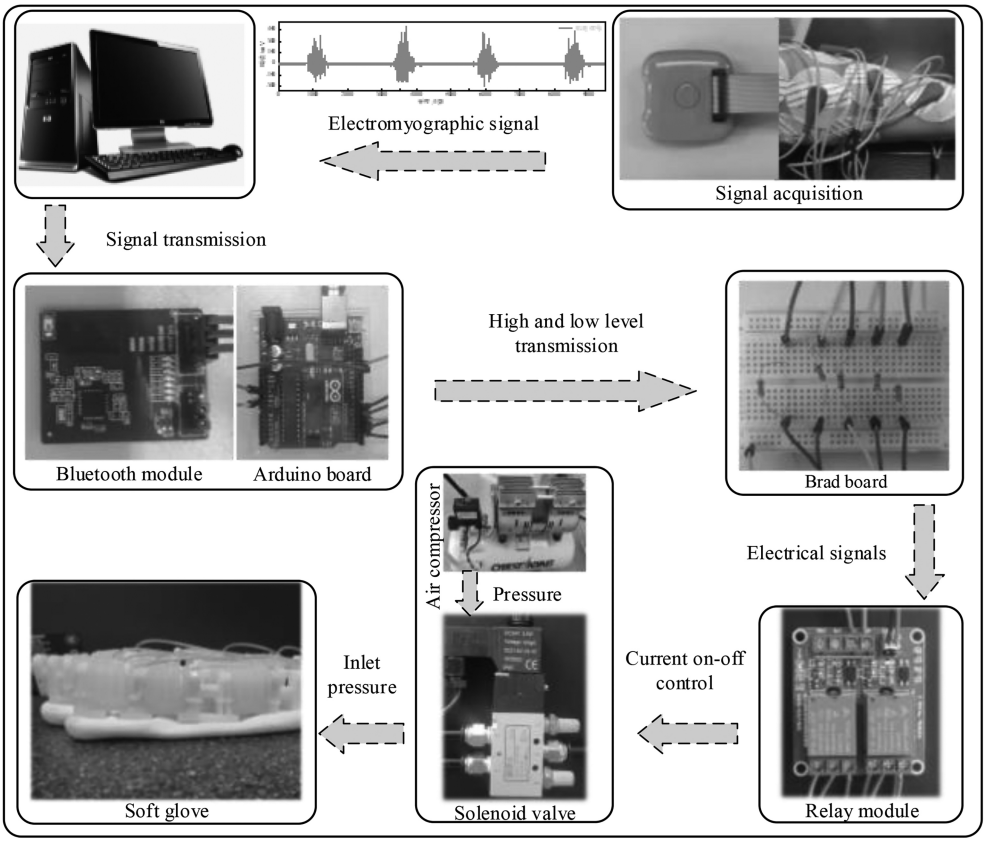


Figure 8. sEMG signal mirror control experimental platform, and the control process of the experimental platform consists of three systems: sEMG signal transmission system, electrical circuit transmission system, and pneumatic circuit system.

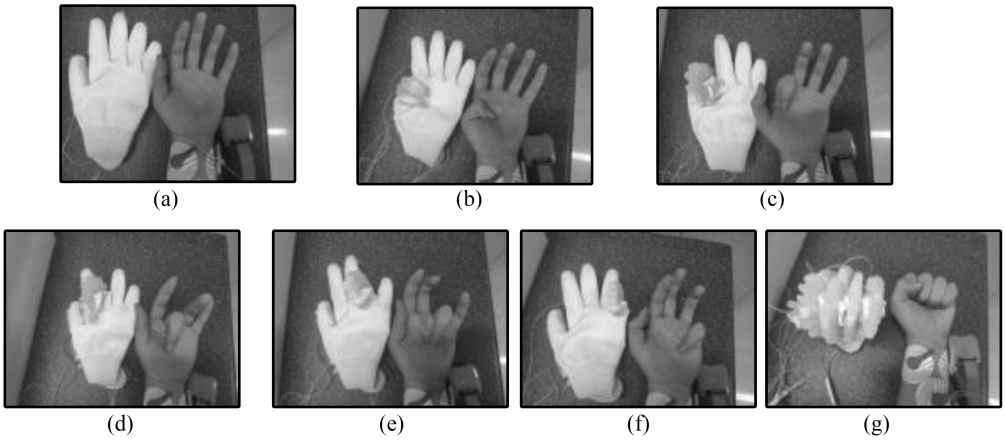


Figure 9. Myoelectric control experiment.

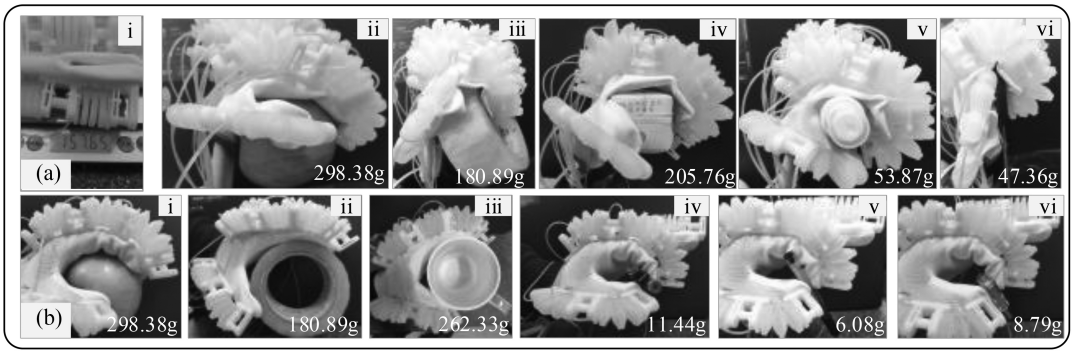


Figure 10. Grasping experiment of soft glove.

## 5. Conclusion

In this paper, a soft glove with multiple parallel joints is designed and made by imitating the skeletal structure of human hands. The soft glove prototype adopts a lightweight design method, with a total weight of 158 g. The static motion simulation and experiment of the soft glove were completed. The mirror therapy is implemented using sEMG, and the patient can realise the synchronous movement of the affected side and the healthy side through the soft glove. The following conclusions were drawn during the study of the soft glove:

1) Soft glove allows a single joint to move independently while also allowing numerous joints to move together. The prototype of the soft glove is realised using the size of human hands and the skeleton structure of human hands, and the feasibility of the proposed structure is verified.
2) By comparing the simulation and experimental results in soft finger static motion, it can be obtained that the average error between simulation and experimental results of MP, PIP, and DIP is 1.21 degrees, 1.4 degrees, and 1.04 degrees, respectively. The maximum error between simulation and experimental results is 1.4 degrees MP, 3.5 degrees PIP, and 2.7 degrees DIP.
3) The output force of the soft actuator can reach 19.83 N when the pressure exceeds 150 kPa. The feasibility of the control system was verified by the sEMG mirror control experiment of the soft glove, and the characteristics of large strain, high grasping force, and flexibility of multi-joint linkage of soft glove were verified by grasping experiments.

## Funding

This work was supported by Scientific and technological breakthroughs in Henan Province (NO. 232102221031) and the Open Project of Henan Key Laboratory of Intelligent Manufacturing of Mechanical Equipment, Zhengzhou University of Light Industry (No. IM202310).

## References

[1] R. Daniela and T. Michael, Design, fabrication and control of soft robots, *Nature, 521*(7553), 2015, 467–475.

[2] Z.Q. Shen, F.F. Chen, X.Y. Zhu, K.T. Yong, and G.Y. Gu, Stimuli-responsive functional materials for soft robotics, *Journal of Materials Chemistry B, 8*(39), 2020, 8972–8991.

[3] H. Banerjee, Z.T.H. Tse, and H.L. Ren, Soft robotics with compliance and adaptation for biomedical applications and forthcoming challenges, *International Journal of Robotics and Automation, 33*(1),2018, 69–80.

[4] Y.L. Yap, S.L. Sing, and W.Y. Yeong, A review of 3D printing processes and materials for soft robotics, *Rapid Prototyping Journal, 26*(8), 2020, 1345–1361.

[5] M.S. Ainla, D.Y. Verma, and GM. Whitesides, Soft, rotating pneumatic actuator, *Soft Robotics, 4*(3), 2017, 297–304.

[6] B. Gorissen, D. Reynaerts, S. Konishi, K. Yoshida, J.-W. Kim, and M.D. Volder, Elastic inflatable actuators for soft robotic applications. *Advanced Materials, 29*(43), 2017, 1604977.

[7] D. Mccoul, S. Rosset, S. Schlatter, and H. Shea, Inkjet 3D printing of UV and thermal cure silicone elastomers for dielectric elastomer actuators, *Smart Material Structures, 26*(12), 2017, 125022.

[8] M. Cianchetti, C. Laschi, A. Menciassi, and P. Dario, Biomedical applications of soft robotics, *Nature Reviews Materials, 3*(6), 2018,143–153.

[9] Y. Kim, E. Genevriere, P. Harker, M. Balicki, S.U. Lee, H.G. Bowman, A.B. Patel, et al, Telerobotic neurovascular interventions with magnetic manipulation, *STROKE, 53*(1), 2022.

[10] M. Wehner, R.L. Truby, D.J. Fitzgerald, B. Mosadegh, G.M. Whitesides, J.A. Lewis, and R.J. Wood, An integrated design and fabrication strategy for entirely soft, autonomous robots, *Nature, 536*, 2016, 451–455.

[11] J.Z. Fan, S.Q. Wang, Q.G. Yu, and Y. Zhu, Swimming performance of the frog-inspired soft robot, *Soft Robotics, 7*, 2020, 615–626.

[12] X. Wang, A. Khara, and C. Chen, A soft pneumatic bistable reinforced actuator bioinspired by Venus flytrap with enhanced grasping capability, *Bioinspiration and Biomimetics, 15*(5), 2020, 056017.

[13] Y.H. Chen, S. Le, Q.C. Tan, O. Lau, F. Wan, and C. Song, A lobster-inspired robotic glove for hand rehabilitation, *Proc. IEEE International Conference on Robotics and Automation,* Singapore, 2017, 4782–4787.

[14] H. Sun, N.Y. Wang, H. Jiang, and X.P. Chen, Flexible Honeycomb PneuNets robot, *International Journal of Robotics and Automation,31*(6),2016 ,475–483.

[15] Y. Kim and X.H. Zhao, Magnetic soft materials and robots, *Chemical Reviews, 122*(5) ,2022,5317–5364.

[16] C.Y. Chu and R.M. Patterson, Soft robotic devices for hand rehabilitation and assistance: A narrative review, *Journal of NeuroEngineering and Rehabilitation, 15*(1), 2018, 9.

[17] Y.H. Kai, L.J. Hoon, N. Fatima, and H.Y. Chen, Design and preliminary feasibility study of a soft robotic glove for hand function assistance in stroke survivors, *Frontiers in Neuroscience, 9*(11), 2017, 547.

[18] W. Kim, J. Byun, J.-K. Kim, W.-Y. Choi, K. Jakobsen, J. Jakobsen, D.-Y. Lee, and K.-J. Cho, Bioinspired dual-morphing stretchable origami, *Science Robotic, 4*(36), 2019, 1–10.

[19] H. Al-Fahaam, S. Davis, and S. Nefti-Meziani, The design and mathematical modelling of novel extensor bending pneumatic artificial muscles (ebpams) for soft exoskeletons, *Robotics and Autonomous Systems, 99*, 2018, 63–74.

[20] S.N. Alibadi and S. Davis, The design, kinematics and torque analysis of the self-bending soft contraction actuator, *Actuators, 9*(2), 2020, 33.

[21] G.C. Arnau, C. Ian, and R.Y.B. Ferdinando, Toward a common framework for the design of soft robotic manipulators with fluidic actuation, *Soft Robotics, 5*(5), 2018, 622–649.

[22] L.L. Yuan, Design and implement of a soft exoskeleton robotic system for hand rehabilitation, *Dissertation, Huazhong University of Science and Technology* Wuhan, Hubei, 2018, 16–21.

## Biographies

*Huadong Zheng* received the B.S. degree in mechanical manufacture and automation from Anyang Institute of Technology, Anyang, China, in 2010, the M.S. degree in mechanical manufacture and automation from Zhengzhou University, Zhengzhou, China, in 2013, and the Ph.D. degree in mechatronic engineering from Dalian University of Technology, Dalian, China, in 2019. He is currently a Lecturer with the School of Mechanical and Electrical Engineering, Zhengzhou University of Light Industry, Henan International Joint Laboratory of Complex Mechanical Equipment Intelligent Monitoring and Control, Henan Provincial Key Laboratory of Intelligent Manufacturing of Mechanical Equipment, China. His research interests are in robot design, industrial robot control, and additive manufacturing.

*Yongfeng Tian* received the B.S. degree in mechanical manufacture and automation from Taiyuan University of Science and Technology, Taiyuan, China, in 2020. He is currently pursuing the M.S. degree in mechanical engineering with the School of Mechanical and Electrical Engineering, Zhengzhou University of Light Industry. He is currently a Member of the Robot Control Research Team, Key Laboratory of Intelligent Manufacturing of Mechanical Equipment in Henan Province, School of Mechanical and Electrical Engineering, Zhengzhou University of Light Industry. His research interests include soft robot, electromechanical control system, and industrial robot control.

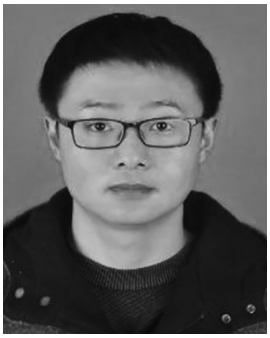

*Yan Cheng* received the B.S. and M.S. degrees in mechanical engineering from Zhengzhou University of Light Industry, Zhengzhou, China, in 2018 and 2021, respectively. He has been a Member of Henan Provincial Key Laboratory of Intelligent Manufacturing of Mechanical Equipment, China. His research interests include soft robot and rehabilitation robot.

*Caidong Wang* received the B.S. degree from the College of Engineering, Northeast Agricultural University, Harbin, China, in 2005, and the Ph.D. degree in mechanical and electrical engineering from Harbin Engineering University, Harbin, China, in 2011. He is currently a Professor with the School of Mechanical and Electrical Engineering, Zhengzhou University of Light Industry, Henan Provincial Key Laboratory of Intelligent Manufacturing of Mechanical Equipment, China. His research interests are in robot design and automatic control.

*Ayong Li* received the B.S. degree in mechanical manufacture and automation from Xinxiang College, Henan, China, in 2021. He is currently pursuing the master's degree in mechanical engineering with the School of Mechanical Engineering, Zhengzhou University of Light Industry. He is currently a Member of the Robot Control Course Group, Henan Key Laboratory of Intelligent Manufacturing of Machinery and Equipment, College of Mechanical and Electrical Engineering, Zhengzhou University of Light Industry. His research interests include biomimetic robot, soft robot, and electromechanical control system.

*Xinjie Wang* received the B.S. and Ph.D. degrees from the School of Mechanical Science and Engineering, Huazhong University of Science and Technology, Wuhan, China, in 1982 and 2005, respectively. She has been a Professor with the School of Mechanical and Electrical Engineering, Zhengzhou University of Light Industry, Henan Provincial Key Laboratory of Intelligent Manufacturing of Mechanical Equipment, China. Her research interests are in robot design and automatic control.

*Fengyang Liu* received the B.S. degree in measurement and control technology and instrumentation from Zhengzhou University of Light Industry, Zhengzhou, China, in 2018, and the M.S. degree in mechanical engineering from Zhengzhou University of Light Industry, Zhengzhou, China, in 2021. He is currently a Lecturer with the School of Electrical and Information Engineering, Zhengzhou University of Light Industry. His main research interests are robotics and machine vision.

*Liangwen Wang* received the B.S. and M.S. degrees from the Department of Mechanical Engineering, Shaanxi University of Science and Technology, Xian, China, in 1983 and 1986, respectively, and the Ph.D. degree from the School of Mechanical Science and Engineering, Huazhong University of Science and Technology, Wuhan, China, in 2012. He is a Professor with the School of Mechanical and Electrical Engineering, Zhengzhou University of Light Industry, Henan Provincial Key Laboratory of Intelligent Manufacturing of Mechanical Equipment, China. His research interests are in robotics and mechanism design.